

Contents lists available at [ScienceDirect](https://www.sciencedirect.com)

Remote Sensing of Environment

journal homepage: www.elsevier.com/locate/rse

Seasonal and long-term variations in leaf area of Congolese rainforest

Yuanheng Sun^{a,b,*}, Yuri Knyazikhin^{a,**}, Xiaojun She^{a,c}, Xiangnan Ni^{a,d}, Chi Chen^{a,e},
Huazhong Ren^b, Ranga B. Myneni^a^a Department of Earth and Environment, Boston University, Boston, MA 02215, USA^b School of Earth and Space Sciences, Peking University, Beijing, China^c School of Geographic Sciences, Southwest University, Chongqing, China^d Department of Earth and Environmental Sciences, Xi'an Jiaotong University, Xi'an, China^e Department of Earth and Environmental Sciences, Lawrence Berkeley National Laboratory, Berkeley, CA 94720, USA

ARTICLE INFO

Keywords:

Leaf area
Remote sensing
Congolese rainforests
Phenology
Long-term trends
MODIS
MISR
DISCOVER EPIC

ABSTRACT

It is important to understand temporal and spatial variations in the structure and photosynthetic capacity of tropical rainforests in a world of changing climate, increased disturbances and human appropriation. The equatorial rainforests of Central Africa are the second largest and least disturbed of the biodiversity-rich and highly productive rainforests on Earth. Currently, there is a dearth of knowledge about the phenological behavior and long-term changes that these forests are experiencing. Thus, this study reports on leaf area seasonality and its time trend over the past two decades as assessed from multiple remotely sensed datasets. Seasonal variations of leaf area in Congolese forests derived from MODIS data co-vary with the bimodal precipitation pattern in this region, with higher values during the wet season. Independent observational evidence derived from MISR and EPIC sensors in the form of angular reflectance signatures further corroborate this seasonal behavior of leaf area. The bimodal patterns vary latitudinally within this large region. Two sub-seasonal cycles, each consisting of a dry and wet season, could be discerned clearly. These exhibit different sensitivities to changes in precipitation. Contrary to a previous published report, no widespread decline in leaf area was detected across the entire extent of the Congolese rainforests over the past two decades with the latest MODIS Collection 6 dataset. Long-term precipitation decline did occur in some localized areas, but these had minimal impacts on leaf area, as inferred from MODIS and MISR multi-angle observations.

1. Introduction

Tropical rainforests play an essential role in modulating regional climate, surface energy partitioning and the Earth's carbon cycle (Chen et al., 2020; Cook et al., 2020). Understanding the spatial patterns and temporal variations and trends in the structure and functioning of rainforests, and the underlying mechanisms and their drivers, is crucial to gaining insights on how these biodiversity-rich and productive ecosystems will respond to future climate change, disturbances and human appropriation (Bi et al., 2015). The seasonal transition between wet and dry seasons is a distinct feature of tropical rainforests, which leads to intra-annual patterns of leaf flushing and abscission (Bi et al., 2015; Samanta et al., 2012). The growth-limiting impact of water deficit on rainforest during the dry season could be alleviated through deep roots and hydraulic redistribution (Oliveira et al., 2005; Pierret et al., 2016).

However, a continued decline in leaf area and photosynthetic capacity attributed to long-term drying may alter forest composition and structure, such as large-scale tree mortality and dominance of drought-tolerant species (Adams et al., 2009; Fauset et al., 2012; Martínez-Vilalta and Lloret, 2016).

Seasonal variations in the Amazonian rainforests has been an active research topic in recent years (Brando et al., 2010; Huete et al., 2006; Morton et al., 2014; Myneni et al., 2007). The community-consensual view is that higher greenness and leaf area appear during the sunlight-rich dry season in well-hydrated Amazonian rainforests (Bi et al., 2015; Brando et al., 2010; Huete et al., 2006; Myneni et al., 2007), even though this view has been questioned (Galvão et al., 2011; Morton et al., 2014). Science questions surrounding the functionality of Amazonian rainforests such as drought induced carbon sink variation and impacts of human interference are at the center of debates nowadays (Aragão et al.,

* Corresponding author.

** Corresponding author at: Department of Earth and Environment, Boston University, Boston, MA 02215, USA.

E-mail addresses: yhsun@pku.edu.cn (Y. Sun), jknjazi@bu.edu (Y. Knyazikhin).<https://doi.org/10.1016/j.rse.2021.112762>

Received 20 December 2020; Received in revised form 6 October 2021; Accepted 16 October 2021

Available online 13 November 2021

0034-4257/© 2021 Elsevier Inc. All rights reserved.

2018; Brienen et al., 2015; Pires and Costa, 2013; Yang et al., 2018b). The equatorial rainforests of Central Africa, the second largest and least disturbed of the biodiversity-rich and highly productive rainforests on Earth (Cook et al., 2020), have attracted less attention compared with its Amazonian counterpart.

The bimodal precipitation pattern (two wet and two dry seasons per year) in the Congo basin controlled by the migration of the tropical rain belt, is much different from that in the Amazon (Jiang et al., 2019; Nicholson, 2018; Raghavendra et al., 2020; Sorf et al., 2017). For all vegetation types within the Congo Basin enhanced vegetation index (EVI) profiles were found to be highly seasonal and strongly correlated to rainfall and to a lesser extent to light regimes (Gond et al., 2013). Two-band enhanced vegetation index (EVI2) from the geostationary Spinning Enhanced Visible and Infrared Imager (SEVIRI) and polar-orbiting Moderate Resolution Imaging Spectroradiometer (MODIS) also revealed similar bimodal seasonal pattern (Yan et al., 2016a). It was found (Yan et al., 2017) that the spatial variation in wet season timing within the Congo Basin exhibited distinct latitudinal gradients whereas the variation in the canopy greenness cycle timing was relatively small. Analyses of MODIS EVI and solar-induced chlorophyll fluorescence (SIF) and fraction of absorbed radiation from the Global Ozone Monitoring Experiment-2 (GOME-2) suggest that an annual rainfall threshold of approximately 2000 mm yr⁻¹ determines whether the supply of seasonally redistributed subsurface water storage from the wet season can satisfy plant water demands in the subsequent dry season; thus water availability exerts a first-order control on photosynthetic seasonality in tropical forests (Guan et al., 2015; Ndehedehe et al., 2019).

Recent studies have also revealed a large-scale and long-term drying trend during the 1979 to 2010 period over the Congolese rainforests in central Africa (Jiang et al., 2019; Raghavendra et al., 2020; Zhou et al., 2014). This has been linked to a shift in tropical Walker circulation (Hua et al., 2018; Hua et al., 2016), intensifying thunderstorm activities (Raghavendra et al., 2018) and Madden-Julian oscillation (Raghavendra et al., 2020). This drying was supposed to have led to a widespread loss in greenness of Congolese forests during 2000 to 2012 as they were claimed to be more sensitive and less resilient to climate change as compared to its Amazonian counterpart (Hirota et al., 2011; Jiang et al., 2019; Zhou et al., 2014). On the other hand, some recent studies based on latest versions of satellite data reported no significant browning signals during the 2000 to 2017 period (Chen et al., 2019; Piao et al., 2020). As such, the question of greening or browning of Congolese rainforests over the past 20 years is still unclear and in debate, especially in the context of increasing drying durations and from the perspective of biophysical parameters. Moreover, a drying climate over the past two decades has been associated with changes in forest composition, leaf phenology and community-level functional traits in tropical forests (Aguirre-Gutiérrez et al., 2020), which requires further explorations.

In addition to climatic factors mentioned above, degradational transitions in land cover and agricultural expansion also drive the vegetation dynamics in rainforests (Costa et al., 2007). Since the Congolese rainforests are less disturbed by human activities compared with other equatorial forests (Cook et al., 2020), the climatic influence is our main focus. This study is focused on exploring the intra-annual seasonality and its controls, inter-annual variability and long-term trends in leaf area of the Congolese rainforests. More specifically, our primary objectives are to (i) document seasonal variation in leaf area of Congolese rainforests and how do seasonal patterns vary latitudinally within this large region; (ii) estimate the sensitivity of leaf area to changes in precipitation for different regions and seasonal cycles; (iii) analyze long-term trends in leaf area; and (iv) assess impact of long-term drying on leaf area and leaf optics. Multiple remote sensing datasets and vegetation proxy metrics are analyzed to achieve our objectives.

Monitoring of dense vegetation such as equatorial rainforests represents one of the most complicated case in optical remote sensing because reflection of solar radiation saturates and becomes weakly sensitive to vegetation changes. At the same time, the satellite data are

strongly influenced by changing sun-sensor geometry. This makes it difficult to discriminate between vegetation changes and sun-sensor geometry effects. As such, the above-mentioned leaf area seasonal variation and long-term greening/browning trends revealed by single-viewing remotely sensed datasets require more evidence. Our secondary objective is to demonstrate value of multi-angle observations to unambiguously detect changes in properties of dense equatorial forests.

2. Materials and methods

2.1. Datasets

Various variables from several independent satellite sensors over the Congo basin were analyzed in this research. These include leaf area index (LAI), normalized difference vegetation index (NDVI) (Rouse et al., 1974), EVI (Liu and Huete, 1995), land cover maps, land surface temperature (LST) and evapotranspiration (ET) from MODIS. Additionally, the following datasets were also utilized in this research: precipitation from Tropical Rainfall Measuring Mission (TRMM), photosynthetically active radiation (PAR) from Clouds and Earth's Radiant Energy System (CERES), surface bidirectional reflectance factor (BRF) and directional hemispherical reflectance (DHR) from Multi-angle Imaging Spectroradiometer (MISR) on the Terra platform and BRF from Earth Polychromatic Imaging Camera (EPIC) on Deep Space Climate Observatory (DSCOVR). Table 1 shows datasets used in this study.

2.1.1. MODIS data

The Terra and Aqua MODIS Collection 6 (C6) 8-day composite LAI products (MOD15A2H and MYD15A2H) for the period of February 2000 to December 2019 were used in this study. The data are at 8-day temporal frequency and projected on a 500-m sinusoidal grid. The C6 MODIS LAI product correctly accommodates structural and phenological variability in all biome types and agree with ground truth data within root mean square error (RMSE) of 0.66 LAI (Yan et al., 2016b; Yan et al., 2016c).

C6 Terra MODIS monthly NDVI and EVI products (MOD13C2) from February 2000 to December 2019 were also used as radiometric measures of vegetation greenness. The NDVI is a vegetation index widely used in many studies of vegetation dynamic. It is calculated as the difference between BRFs at near-infrared (NIR) and red spectral bands normalized by their sum. The EVI is calculated as the difference between BRFs at NIR and red spectral bands normalized by a linear combination of BRFs at blue, red and NIR bands. It was found especially useful for monitoring vegetation in high biomass tropical broadleaf forests (Brando et al., 2010; Xu et al., 2011; Zhou et al., 2014). The C6 MOD13C2 product is projected on a 0.05° geographic Climate Modelling Grid (CMG) (Huete et al., 2002). In addition, monthly gridded Collection 5 (C5) MODIS NDVI/EVI product (MODVI) from February 2000 to December 2012 in CMG 1° resolution was also used in our study for

Table 1
Brief information of variables and datasets used in this study.

Variable	Product	Spatial resolution	Temporal resolution
LAI	C6 MOD15A2H & MYD15A2H	500 m	8 day
EVI	C6 MOD13C2	0.05°	monthly
NDVI	C5 MODVI	1°	monthly
Land cover	C6 MCD12C1	0.05°	yearly
LST	C6 MYD11C3	0.05°	monthly
Evapotranspiration	C6 MOD16A2	500 m	8 day
Precipitation	TRMM	0.25°	monthly
PAR	CERES	1°	monthly
BRF	Terra MISR	1.1 km	16 day
DHR	Terra MISR	1.1 km	16 day
BRF	DSCOVR EPIC	10 km	65 to 110 min

comparisons.

C6 Terra and Aqua MODIS land cover product (MCD12C1) from 2001 to 2019 at yearly intervals and at a 0.05° spatial resolution was used to identify our study area. Maps of several classification schemes are available in the MCD12C1 dataset (Friedl et al., 2002). The map of LAI classification scheme was adopted in this research (Supplementary Information Fig. S1).

Daytime LST from C6 Aqua MODIS (MYD11C3) for the period July 2002 to December 2019 was used to quantify temperature variations related to changes in leaf area and other climate variables. MYD11C3 measures the temperature of Earth's surface thermal emission at local time ~ 13:30, which is believed to provide the largest LST contrast between vegetated and non-vegetated surfaces compared to other MODIS LST measurements. Monthly LST values from the MYD11C3 product are derived by compositing and averaging values from the corresponding month of MYD11C1 daily files, and projected on a 0.05° CMG grid (Wan, 2014).

The Terra MODIS C6 8-day composite evapotranspiration product (MOD16A2) projected on a 500-m sinusoidal grid from January 2000 to December 2019 was used to quantify climatic water deficit variations. The algorithm used to generate MOD16A2 is based on the logic of the Penman-Monteith equation, which includes inputs of daily meteorological reanalysis data along with other MODIS products such as vegetation property dynamics, albedo, and land cover (Mu et al., 2007; Mu et al., 2011).

2.1.2. TRMM precipitation and CERES PAR fluxes

Monthly precipitation data from the TRMM (3B43 version 7) at 0.25° spatial resolution for the period January 2000 to December 2019 was used in this study. The 3B43 version 7 TRMM data provides the best-estimate precipitation rate and root-mean-square precipitation-error estimates by combining four independent precipitation fields (Huffman et al., 2007). Monthly at-surface all-sky downward PAR, calculated by summarizing direct and diffuse PAR fluxes from CERES (SYN1deg_L3 product) at 1° resolution for the period of March 2000 to November 2019 was used (Rutan et al., 2015).

2.1.3. Terra MISR and DSCOVR EPIC data

Level 2 land surface and aerosol products from MISR (version 3) for the period of January 2000 to December 2019 were used in this study. The MISR sensor views the Earth's surface with nine cameras simultaneously and enables direct measurements of angular variation of forest reflected radiation over a wide range of the phase angle that the single-viewing sensors (e.g., Terra and Aqua MODIS) can provide only in very limited cases (Bi et al., 2015; Song et al., 2018). MISR has a ground track repeat cycle every 16 days and achieves global coverage every 9 days. The surface reflectances, DHR and BRF, are at 1.1 km spatial resolution. The aerosol optical depth (AOD) is available at 4.4 km spatial resolution. The surface and aerosol products are projected on Space Oblique Mercator (SOM) projection, in which the reference meridian nominally follows the spacecraft ground track. The land surface product provides BRF at nine MISR view angles (nadir, ±26.1°, ±45.6°, ±60.0° and ±70.5°) in four spectral bands (446, 558, 672, and 866 nm). The MISR view directions form "view" lines on the polar plane (Supplementary Information Fig. S2). Each view line sees a certain part of the MISR 360 km swath.

Level 2 Multi-Angle Implementation of Atmospheric Correction (MAIAC) surface BRF retrieved from DSCOVR EPIC observations from 2016 to 2019 was also used. The EPIC instrument provides imageries in near backscattering directions with the phase angle between 4° and 12° at ten ultra-violet to NIR narrow spectral bands. This feature complements MISR observations since it extends MISR angular sampling to the near backscattering directions. The MAIAC BRF are available at four spectral bands; they are 443, 551, 680 and 780 nm. Data are projected on a 10-km sinusoidal grid and available at 65 to 110 min temporal frequency.

2.2. Data processing

This study was focused on structurally intact and undisturbed region of Congolese tropical moist broadleaf forests in Central Africa (5°N-6°S, 14°E-31°E), which were defined as a region with no changes in land cover type during the 2000 to 2019 period. First, evergreen broadleaf forest pixels in the LAI classification scheme at 0.05° resolution for which no land use/cover change was detected during the 2000 to 2019 period were selected. Second, the binary 0.05° evergreen broadleaf forest images were spatially aggregated into a 0.25° coarser resolution map to match the spatial resolution of rainfall TRMM dataset. Pixels at 0.25° resolution were labeled as rainforest only if at least 80% of its 0.05° sub-pixels (i.e., 20 in 25 sub-pixels) were forested. Third, those isolated pixels in the Congolese forest border were removed at 0.25° mask map to minimize human impact. The 1653 pixels at 0.25° resolution identified by this procedure were considered as structurally intact and undisturbed forests.

All vegetation and climate variables were selected using flags indicating highest retrieval quality. The 8-day 500 m LAI products from Terra (MOD15A2H) and Aqua (MYD15A2H) MODIS sensors were used to generate monthly average LAI values. The cloud contaminated pixels were removed. Only the best quality LAI values generated using main algorithm were used in our analyses. The monthly LAIs were then spatially aggregated onto a 0.05° CMG grid (Chen et al., 2019). The evapotranspiration data used in our study was generated by selecting best-quality retrievals in the MODIS C6 ET product first and then degraded to 0.05° CMG monthly composites following the same procedure used to obtain LAI dataset. The LAI and NDVI/EVI were further refined by removing low quality data by consulting NDVI/EVI quality assurance (QA) flags. We selected highest quality LST based on LST QA. The LAI, NDVI/EVI, ET and LST datasets over intact and undisturbed region of the Congolese forests were then spatially aggregated to 0.25° resolution. During the process of spatial aggregation, only pixel whose sub-pixels are all valid was retained. Climatic water deficit (CWD) was calculated as the difference between potential evapotranspiration and actual evapotranspiration from the ET dataset. Nearest neighbor interpolation was adopted to resample data to 0.25° for the C5 NDVI/EVI and CERES PAR dataset at a spatial resolution coarser than 0.25°.

The MISR surface BRF and DHR were first refined by removing pixels with AOD over 0.3. EPIC images at local solar time around 10:30 am were used in our analyses, which were also refined by removing pixels with AOD over 0.3. MISR and EPIC datasets were further re-projected to 0.01° and 0.1° CMG grids, respectively. We expressed BRF and DHR values in a coordinate system with the polar axis pointed towards the Sun. The view zenith angle in this "sun-tracking" coordinates was given by the phase angle, γ , i.e. the angle between the directions to the sun and sensor and calculated as:

$$\gamma = \arccos[\cos SZA \cos VZA + \sin SZA \sin VZA \cos(SAA - VAA)] \quad (1)$$

where SZA, VZA, SAA, VAA are solar zenith angle, view zenith angle, solar azimuthal angle and view azimuthal angles (Bi et al., 2015). We assigned the sign "plus" to the phase angle if the direction to the MISR sensor approached the direction to sun from North, and "minus" otherwise (Supplementary Information Fig. S2). In our sun-tracking coordinate system, the MISR BRF was a function of SZA, phase angle and MISR view line, the latter specified by VZA of the MISR nadir camera.

Monthly BRFs and DHRs accumulated over the 20-year period (2000 to 2019) were used to analyze seasonal variation of forest canopy reflectance. For each month, a median BRF value at each phase angle was calculated using all 20-year (2000 to 2019) valid observations of a given pixel in our study area. Histograms of valid MISR spectral DHR at each SZA accumulated over the 20-year period (2000 to 2019) were calculated for each pixel. The most probable values were used to represent spectral DHR of regions as a function of SZA. For analysis of interannual changes, we used median BRFs over the period of

2000–2002 and 2017–2019 to represent the start and the end period, respectively.

2.3. Interpretation of forest BRF

Reflectance of dense vegetation such as the Congolese forests saturates and becomes weakly sensitive to vegetation changes. At the same time, the satellite data are strongly influenced by changing sun-sensor geometry. This makes it difficult to discriminate between vegetation changes and effects of sun-sensor geometry. This section provides an overview of a new approach to detect changes in properties of dense vegetation using angular distribution of forest reflected radiation as a source of diagnostic information. This methodology will be used in Section 3.1 and Section 3.4 to corroborate seasonal and long-term variation in leaf area.

In the case of vegetation canopies with a dark background or sufficiently dense vegetation where the impact of the canopy background is negligible, the BRF can be approximated as (Knyazikhin et al., 2013):

$$\text{BRF}_\lambda(\Omega_0, \Omega) = \frac{\rho(\Omega_0, \Omega)i_0}{1-p} \times \frac{\omega_\lambda(1-p)}{1-p\omega_\lambda} \quad (2)$$

The first factor on the right-hand side of Eq. (2), $\rho(\Omega_0, \Omega)i_0/(1-p)$, is the Directional Area Scattering Factor (DASF), which describes the canopy BRF if the foliage does not absorb radiation. The second factor, $\omega_\lambda(1-p)/(1-p\omega_\lambda)$, is the Canopy Scattering Coefficient (CSC), i.e., the fraction of intercepted radiation that has been reflected from, or diffusively transmitted through, the vegetation. Unlike canopy reflectance and transmittance, the CSC quantifies scattering event per unit leaf surface and therefore conveys information about leaf optical properties. Here Ω_0 (SZA, SAA) and Ω (VZA, VAA) are unit vectors directed from target to the sun and sensor, respectively; i_0 is the canopy interceptance defined as the portion of photons from the incident solar beam that collide with foliage elements for the first time. The symbol ρ designates the directional escape probability, i.e., the probability by which a photon scattered by a foliage element will exit the vegetation in the direction Ω through gaps. Spherical integration of $\pi^{-1}\rho \cdot \cos(\text{VZA})$ results in $1-p$, where p is the recollision probability, defined as the probability that a photon scattered by a foliage element in the canopy will interact within the canopy again (Yang et al., 2017). Finally, ω_λ is the wavelength dependent leaf albedo, i.e., the fraction of radiation incident on a leaf surface that is reflected or transmitted (Huang et al., 2007; Knyazikhin et al., 2011; Wang et al., 2003). We used Eq. (2) to interpret the BRF of Congolese forests. A short summary of its key properties is given below.

The spectrally invariant DASF is a function of canopy geometrical properties, such as the tree crown shape and size, spatial distribution of trees on the ground, and within-crown foliage arrangement (Knyazikhin et al., 2013). Since our study is focused on structurally intact and undisturbed region of the Congolese forests (i.e., no changes in forest geometry), only variation in leaf area can cause variation in DASF. At a given SZA, DASF increases with LAI in all phase angles. At a given LAI, the DASF exhibits a sharp increase as phase angle tends to zero and reaches its maximum value in the retro-illumination direction. This phenomenon is known as the hot spot effect. Increasing SZA with constant LAI results in an asymmetric transformation of the DASF, i.e., increase in its magnitude in backscattering directions, and changes in the range of DASF variations for positive and negative phase angles. This asymmetric transformation also can cause the two DASF signatures to intersect. More details about the effects of changing SZA and LAI on BRF can be found in (Bi et al., 2015).

The spectrally varying CSC is a function of the recollision probability and leaf optics. It increases with the leaf albedo: the more the leaves scatter, the brighter the canopy. As the recollision probability increases with LAI, an increase in LAI triggers an opposite tendency: more photon-foliage interactions and consequently a higher chance for photon to be absorbed. This tends to lower CSC. Such variations trigger a competing

process: increase in LAI tends to darken the vegetation while increase in leaf albedo suppresses it. Note that DASF increases with LAI. This not only compensates for a decrease in the CSC but also makes the BRF an increasing function with respect to leaf albedo and LAI.

The leaf albedo is close to unity, $\omega_\lambda \sim 1$ at weakly absorbing wavelengths such as NIR. In the case of dense vegetation, the recollision probability saturates and become weakly sensitive to LAI. In many instances, variation in LAI with leaf albedo unchanged cannot explain the magnitude of observed variation in CSC under the reflectance saturation conditions. Leaf albedo becomes a key parameter that controls changes in the CSC. A detailed mathematical analysis of variation in the CSC when LAI and leaf albedo vary simultaneously can be found in (Samanta et al., 2012).

The leaf albedo is close to zero, $\omega_\lambda \sim 0$ at strongly absorbing wavelengths. The contribution of multiple scattered photons to BRF and CSC is negligible. A decrease in LAI while holding leaf optics constant necessarily causes a decrease in BRF. The lack of BRF decrease indicates an increase in leaf albedo. Clearly this is also true for DHR, which is just hemispherically integrated BRF. We will use this property to detect changes in leaf albedo.

We followed a methodology documented in (Marshak and Knyazikhin, 2017; Song et al., 2018) to approximate DASF. In this approach, the green and NIR wavelengths are used. Given the BRF at these two wavelengths, the estimate DASF is as:

$$\text{DASF} = \frac{\text{BRF}_{\text{green}} \text{BRF}_{\text{NIR}}}{\text{BRF}_{\text{green}} - \beta(\text{BRF}_{\text{NIR}} - \text{BRF}_{\text{green}})} \quad (3)$$

Here $\text{BRF}_{\text{green}}$ and BRF_{NIR} are BRF at green and NIR wavelengths, $\beta = (1 - \omega_{\text{NIR}})\omega_{\text{green}}/(\omega_{\text{NIR}} - \omega_{\text{green}})$, and ω_{green} and ω_{NIR} stand for leaf albedo at green and NIR spectral bands. DASF defined by Eq. (3) does not vary with variation in ω_{green} and ω_{NIR} as long as canopy structure remains unchanged. We used the leaf level albedo of the brightest leaf, whose values at green and NIR spectral bands were $\omega_{555} = 0.472$, $\omega_{865} = 0.978$ for MISR and $\omega_{551} = 0.490$, $\omega_{779} = 0.979$ for EPIC. These values were obtained from Lewis and Disney's approximation (Lewis and Disney, 2007) of the PROSPECT model (Féret et al., 2008) with the following parameters: chlorophyll content of $16 \mu\text{g cm}^{-2}$; equivalent water thickness of 0.005 cm^{-1} , and dry matter content of 0.002 g cm^{-1} . It was shown that retrieval of DASF using this methodology is weakly sensitive to the uncertainties in the spectral properties of the atmospheric optical depth above the canopy, and the spectral CSC is very sensitive to the presence of chlorophyll in the scene (Marshak and Knyazikhin, 2017).

2.4. Correlation and trends analysis

Correlation of monthly average leaf area and the corresponding climatic variables (e.g., precipitation, PAR) was assessed using Pearson's correlation coefficient. Trends in seasonal average variables (e.g., LAI) for the period of 2000 to 2012 and 2000 to 2019 were evaluated by ordinary least square (OLS) regression test using noise-removed dataset, and the trends with $P \leq 0.1$ were considered as statistically significant in this study to make our results comparable with those reported in (Zhou et al., 2014).

3. Results

3.1. Seasonal variation of leaf area and leaf optics

Monthly precipitation data over the Congolese forests show a bimodal variation that suggests two wet and two dry seasons during the year. It varies between its maximum of about 219 mm in October and the minimum of about 86 mm in January (Fig. 1). The wet seasons occur in March-April-May (MAM, wet season 1) and September-October-November (SON, wet season 2), while dry season months are December-January-February (DJF, dry season 1) and June-July-August (JJA, dry

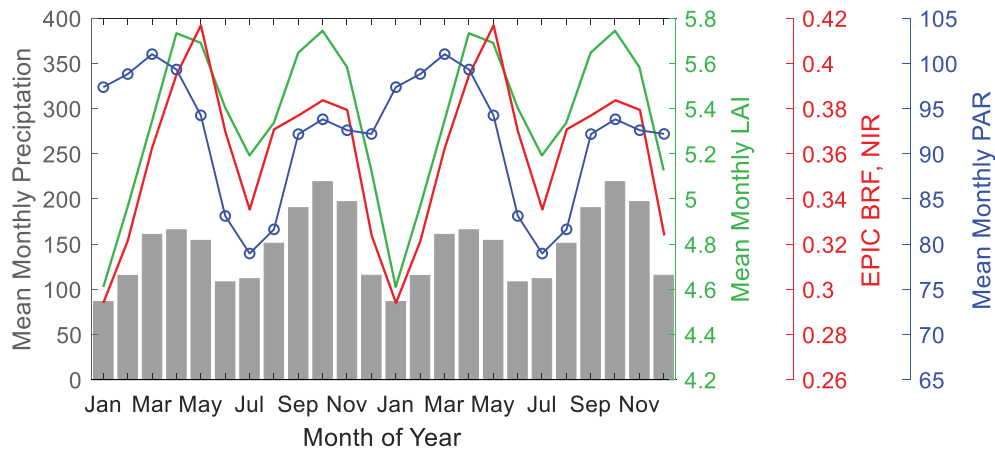


Fig. 1. Annual course of monthly-average precipitation, PAR, LAI, EPIC NIR BRF over the Congolese forests. The annual cycle is repeated two times for better demonstration. Precipitation, LAI and NIR BRF clear show bimodal variations with peaks in March-April-May (MAM, wet season 1) and September-October-November (SON, wet season 2).

season 2) (Fig. 1 and Supplementary Information Fig. S3a). The PAR data exhibit a quasi-bimodal pattern, although somewhat less distinctly: clear-cut variations from December to October and a weak oscillation from October to December (Fig. 1 and Supplementary Information Fig. S3). The sub-seasonal cycle 1 from December to May (dry season 1 and wet season 1) shows less precipitation and more PAR, while cycle 2 from June to December has more precipitation and less PAR (Fig. 1 and Supplementary Information Fig. S3). Monthly average LAI and EPIC NIR BRF data over the Congolese forests also exhibit notable bimodal seasonal variations, which follow the patterns of precipitation (Fig. 1 and Supplementary Information Fig. S3a and b). LAI varies between its maximum of about 5.7 during the wet seasons and a dry season minimum of about 4.6.

Congolese forests can be further divided into four phenological regions based on normalized 20-year mean monthly climatology of precipitation, PAR and LAI using a K-means clustering method, which is an unsupervised measure to find similar features from multiple inputs (Celik, 2009; Xu et al., 2015). We use the four-cluster partition in this study because clusters are big enough to accumulate valid data for statistical analyses and their respective homogeneities are preserved (Fig. 2). Other numbers of clusters are also tested to find an optimal partitioning, and all clusters were generally parallel to the Equator (Supplementary Information Fig. S4), likely because the seasonality of these forests is mainly controlled by the migration of the tropical rain belt and variation of solar radiation along the latitude. Distinct seasonal patterns of climatic and vegetation variables are clearly seen in all

phenological regions across the Congo Basin (Fig. 3). The amplitude of all variables tends to increase from region 1 (north) to region 3 (south) between March and October, which makes the bimodality more distinct. The highland forest (region 4) is characterized by lower LAI values and higher rainfall compared to its lowland counterparts, which is typical of montane forests. The EPIC sensor likely sees different slopes of the mountains; hence the NIR BRF is somewhat less synchronized with LAI compared to other regions. We exclude this region from further analyses given its smaller areal extent and specific character.

Spectrally invariant DASf is a function of canopy geometrical properties, such as the tree crown shape and size, and leaf area density within the canopy. The DASf derived from MISR and EPIC observations of selected regions during wet and dry seasons are different (Fig. 4, left Panels), showing a districting decrease in all directions from wet (October, November) to dry (January) seasons. Such a downward shift in DASf can only result from a negative change in LAI because other structural variables, such as tree crown shape and size do not vary seasonally in our forests. BRF at NIR spectral band exhibits similar behavior: a decrease in reflected radiation in all directions from October (November) to January (Supplementary Information Fig. S5), which suggests more green leaves during the wet season. The CSC shows an opposite tendency, i.e., a positive increase between wet and dry seasons at all spectral bands (Fig. 4, right panels). The decline in LAI is one reason for the observed increase (Section 2.3). A change in leaf albedo is another reason that can impact this coefficient (Section 2.3). Decrease in leaf albedo lowers the CSC value whereas its increase results in the positive change of the CSC value. The question then arises whether one can detect changes in the leaf albedo given changes in the CSC.

A reduction of leaf area tends to decrease forest canopy reflectance (BRF and consequently DHR). At strongly absorbing red (672 nm) wavelength, however, the DHR has increased between wet and dry seasons from 0.014 to about 0.024 in regions 1 and 2 and from 0.015 to 0.018 in region 3 (Fig. 4, left panels). This increase in DHR with decreasing LAI necessarily indicates an increase in leaf albedo (Section 2.3). This also takes place for strongly absorbing blue (446 nm) and moderately absorbing green (551 nm) wavelengths: no decrease in DHR from wet to dry season. This suggests an increase in leaf albedo at visible spectral bands. At NIR (866 nm) wavelength, forest canopy reflectance and CSC show opposite tendencies, namely, BRF (and DHR) decrease whereas CSC increases between wet and dry seasons. Similar tendencies were documented for the Amazonian rainforests (Köhler et al., 2018) and for sufficiently dense broad- and needleleaf forests in the USA (Knyazikhin et al., 2013). A decrease in LAI (and consequently, the recollision probability) tends to increase the CSC (Section 2.3). Under saturation conditions, however, the change in the recollision probability

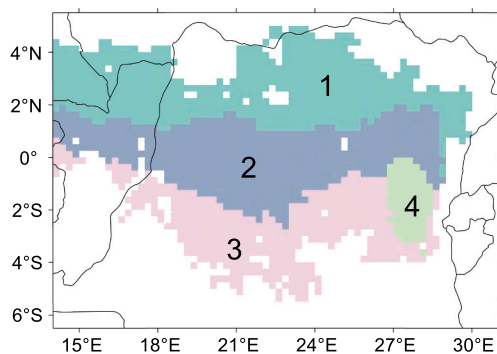


Fig. 2. Four phenological regions clustered based on normalized 20-year mean monthly climatology of precipitation, PAR and LAI data using K-Means clustering method. Region 4 (0.2°S-3°S, 26.8°E-28.5°E) represents montane forests located at moderate elevations between 530 m and 1728 m.

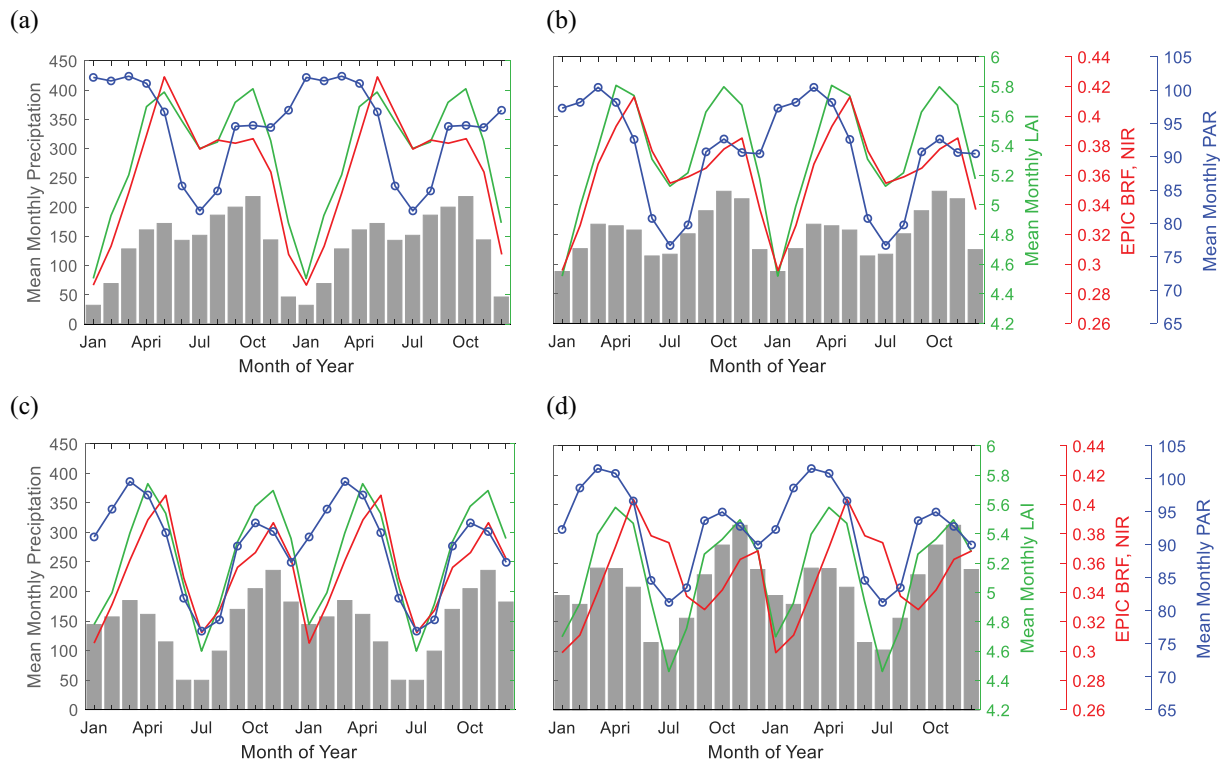


Fig. 3. Annual course of monthly-average precipitation, PAR, LAI, EPIC NIR BRF over (a) region 1, (b) region 2, (c) region 3 and (d) region 4. Phenological regions are shown in Fig. 2. The annual cycles are replicated two times for better demonstration. The peak-to-peak amplitude of bimodal curves tends to increase from north (region 1) to south (region 3).

is negligible. The observed variation in CSC is therefore likely due to a positive change in the leaf albedo.

The sensitivity analyses based on the PROSAIL model (Jacquemoud et al., 2009) suggest that under saturation conditions ($LAI > 4$), the scattering coefficient is nearly insensitive to variations in LAI and SZA (Supplementary Information Fig. S6, panels a and b). The observed changes in the CSC between wet and dry seasons therefore are not due variation in LAI and SZA. In the spectral interval between 450 nm and about 750 nm, chlorophyll is the dominant pigment that absorbs radiation primarily in the blue and red regions of the spectrum, less in the green and essentially none in NIR. This feature makes the CSC sensitive to its concentration in the green and flat in NIR spectral bands (Supplementary Information Fig. S6, panel c). The chlorophyll absorption spectrum declines rapidly with wavelength near the red spectral region and vanishes at about 770 nm, resulting in a sharp jump in the spectrum of leaf albedo from its minimum to a plateau around 800 nm. The magnitude of this plateau is controlled by the amount of dry matter. This imparts sensitivity of the NIR CSC to the concentration of dry matter (Supplementary Information Fig. S6, plot d).

In summary, seasonal variation of leaf area in Congolese forests covaries with the bimodal precipitation pattern, with higher values during the wet seasons. The bimodal pattern is different in the three identified regions, with its bimodality more distinct from the south to the north. The canopy scattering coefficient exhibits an opposite tendency: its value increases from wet to dry and decreases from dry to wet seasons. These variations can be linked to variation in the concentrations of chlorophyll and/or dry matter in green leaves.

3.2. Sensitivity of leaf area to changes in precipitation

Pearson's correlation coefficients between monthly average precipitation, PAR and LAI for the identified regions (Fig. 2) and seasonal periods are shown in Table 2. With the exception of region 3 and

seasonal cycle 1, a significant positive correlation between precipitation and LAI is observed. Moreover, the time series of 20-year monthly precipitation and LAI over the Congolese forests are also significantly positively correlated ($R = 0.67$, $P < 0.01$, Supplementary Information Fig. S7). Such correlations between LAI and PAR ($P < 0.01$) are found in regions 1 to 3 during the cycle 2 (June through November) and in region 3 during the cycle 1 (December through May). These variables are negatively correlated ($P < 0.1$) in region 1 during cycle 1 (Table 2).

We estimate the sensitivity, $\Delta LAI / \Delta \text{precipitation}$, of monthly LAI to changes in precipitation for different regions and seasonal cycles using the slopes of linear regressions. The overall sensitivity of LAI to changes in precipitation varies between regions and depends on the seasonal cycle. It tends to decrease from north to south for the full seasonal cycle (December to November) (Fig. 5a). The regions show weak variation of the sensitivity within seasonal cycles (cf. Fig. 5b and c). LAI exhibits a stronger response to changes in the precipitation during the seasonal cycle 1 (December to June). This difference is due to very different distributions of precipitation, PAR and climatic water deficit during cycles 1 and 2 (Supplementary Information Fig. S8). More precipitation occurs in cycle 2 than in cycle 1, causing a higher climatic water deficit. Thus, LAI in our forests is more sensitive to the changes in precipitation during cycle 1.

3.3. Long-term trends in leaf area

A widespread decline in Congolese rainforest greenness over the 2000–2012 period has been recently reported (Jiang et al., 2019; Raghavendra et al., 2020; Zhou et al., 2014). This result however was questioned, suggesting no significant browning signal in the 2000 to 2017 period (Chen et al., 2019; Piao et al., 2020). These contradictory results justify a re-examination of the long-term trend in greenness of the Congolese forests. Here, we reproduce linear trends in C5 EVI and precipitation in April-May-June for the 2000 to 2012 period as reported in

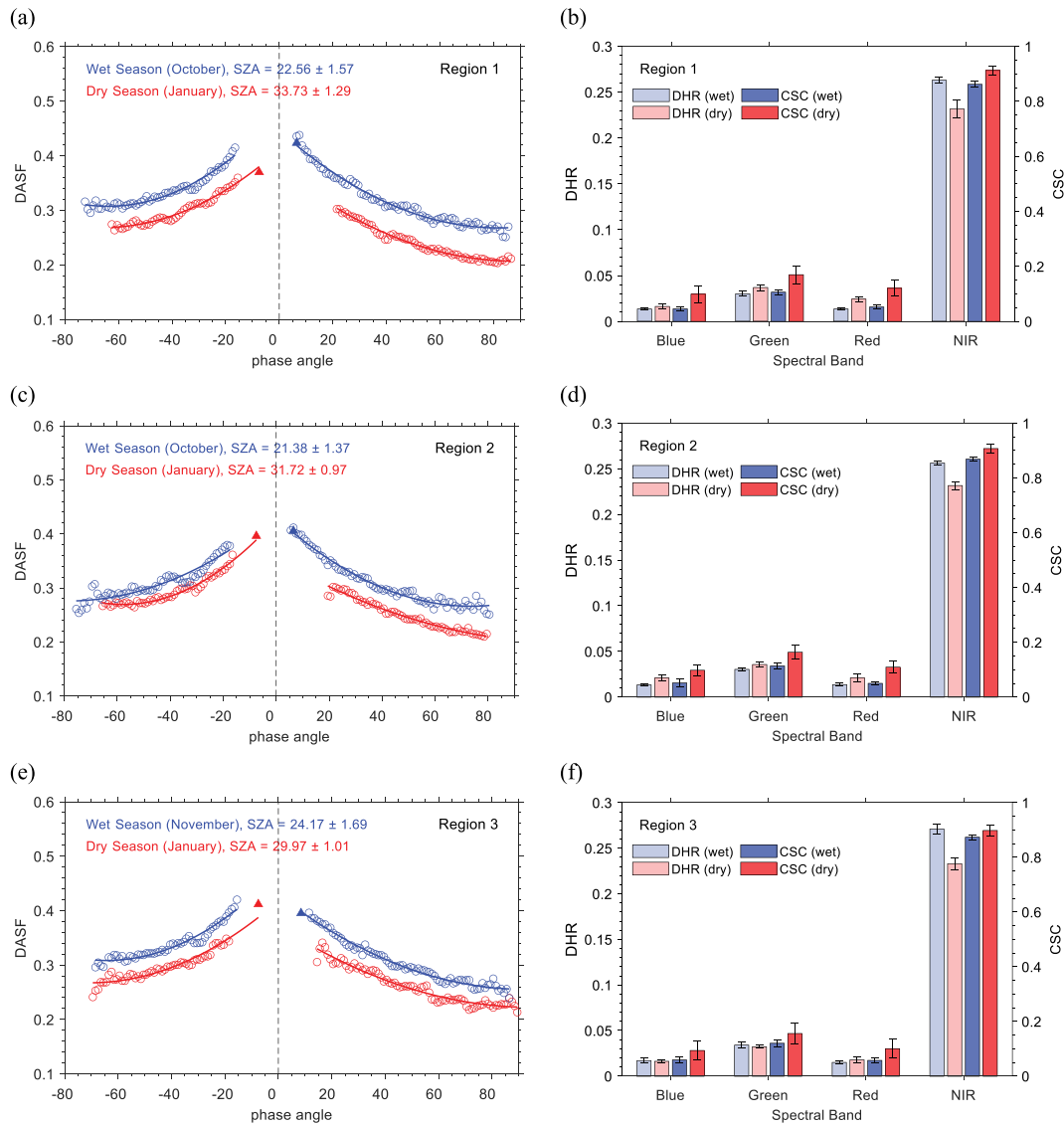


Fig. 4. Directional Area Scattering Factors (DASF) derived from MISR and DSCOVR EPIC data (left panels), MISR Directional Hemispherical Reflectances (DHR) and Canopy Scattering Coefficients (CSC) during wet and dry seasons over region 1 (panels a and b), region 2 (panels c and d) and region 3 (panels e and f). The circles and solid triangles represent MISR and DSCOVR EPIC observations. The lines show polynomial fits to MISR data. There were no enough valid reflectance data over region 3 in October. Therefore, we use November to represent the dry season in this region.

Table 2

Pearson’s correlation coefficients of regional mean monthly LAI and precipitation and PAR over different region and different seasonal cycle. (*P < 0.1, **P < 0.01).

		Cycle 1	Cycle 2	annual
R (TRMM, LAI)	Entire region	0.68**	0.59**	0.63**
	Region 1	0.81**	0.41**	0.78**
	Region 2	0.58*	0.55**	0.56**
	Region 3	0.13	0.65**	0.48**
	Entire region	0.01	0.67**	-0.01
R (PAR, LAI)	Region 1	-0.17*	0.46**	-0.29**
	Region 2	-0.07	0.64**	0.07
	Region 3	0.25**	0.73**	0.52**

(Zhou et al., 2014) and for an extended period of 2000 to 2019 first, and then generate linear trends in C6 EVI, NDVI and LAI for the same periods.

The MODIS C5 EVI declines over 98% of the study area, with 54% showing a significant negative trend (P < 0.1) (Fig. 6a). TRMM

precipitation declines over 77% of the area with 13% indicating significant change with P < 0.1 (Fig. 6b). These results suggest decrease in rainfall and widespread decline in Congo rainforest greenness from 2000 to 2012. Note that “drying area” is reduced from 77% to 63% (13% to 5% with P < 0.1) for the period of 2000 to 2019.

The widespread decline of Congo rainforest greenness in the 2000 to 2012 period has disappeared in the latest Collection 6 MODIS data (Fig. 6, middle panels). Our re-analyses suggest declines in EVI, NDVI and LAI over 43% to 51% of the study area with only 2% to 5% showing significant negative trends (P < 0.1). For the longer period (2000 to 2019), the browning areas have been reduced to 19%–42%, with a negative trends below 4% (P < 0.1) (Fig. 6, lower panels). The difference in the trends is attributable to Terra MODIS sensor degradation found in C5 data (Wang et al., 2012; Zhang et al., 2017).

The regional mean precipitation and PAR over 20 years do not show significant positive or negative trends for all seasons across the Congo basin because of strong interannual variability (Supplementary Information Fig. S9). The regional mean LAI, however, increases by 0.0865 (P = 0.0168) per decade during wet season 1 (March to May) from 2000

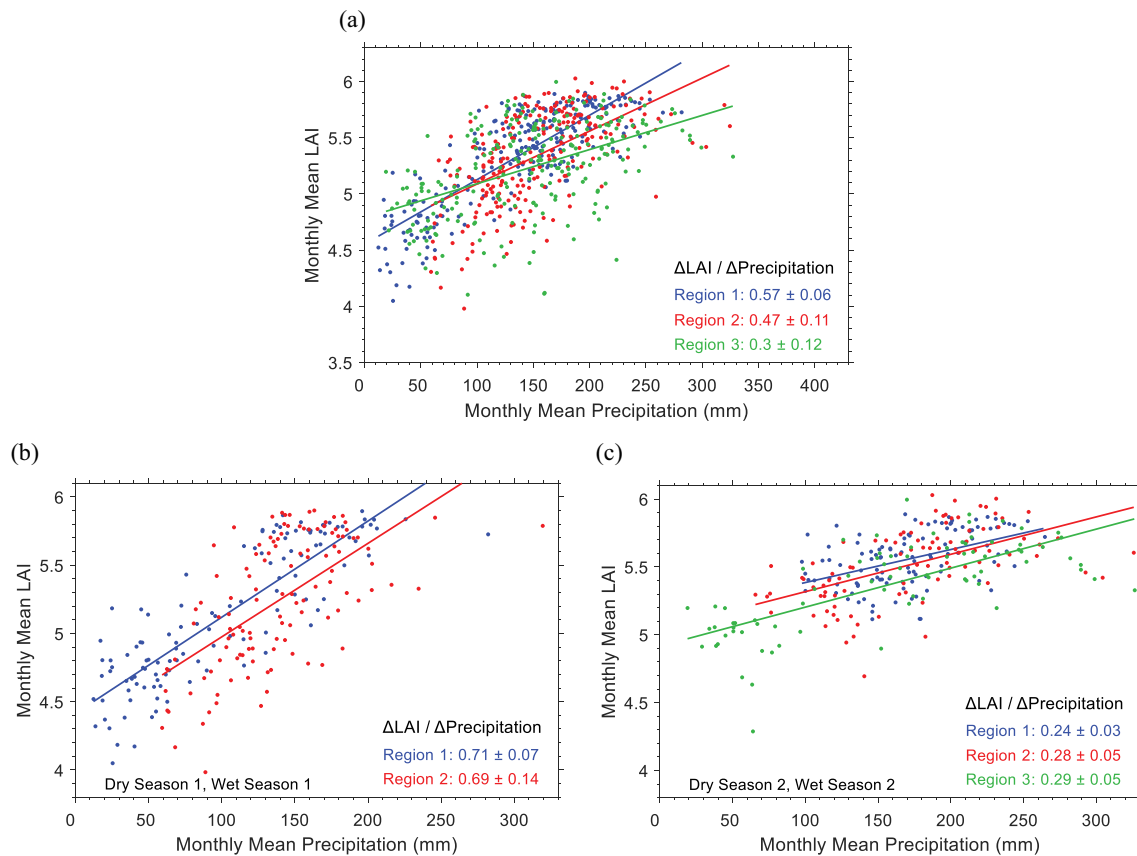


Fig. 5. Relationship between regional monthly precipitation and LAI during (a) full annual seasonal cycle, (b) seasonal cycle 1 (December–May) and (c) cycle 2 (June–November). Slopes of the regression lines are taken as a measure of LAI sensitivity to changes in in the precipitation ($\Delta\text{LAI}/\Delta\text{Precipitation}$).

to 2019 (Supplementary Information Fig. S9b), and the leaf area trends are also positive but not significant for the other wet or dry seasons (Supplementary Information Fig. S9a, c, d).

3.4. Impact of drying trends on leaf area and leaf optics

Here we focus on a South-East part (0.5°N – 2.5°S , 25.5°E – 28.5°E) of our study area, where a significant precipitation decline is observed (Figs. 7a and b), with the goal of understanding the impact of this event on changes in forest structure and leaf optics.

With the exception of NDVI in the dry season 2 (June to August), no significant decline or increase in trends in regional mean NDVI, EVI and LAI over the past two decades are detected. The time series of LAI and EVI are found to be strongly correlated with $R = 0.56$ ($P < 0.01$) in wet season 1 (MAM) and $R = 0.74$ ($P < 0.01$) in dry season 2 (JJA).

Next, we examine MISR BRFs at NIR (866 nm) spectral band over the region with significant drying happened during the early (2000–2002) and later (2017–2019) part of the 20-year observation period. Reflectance in April (wet season) and June (dry season) are under almost identical observation and illumination conditions (Fig. 8 left panels). No significant differences in magnitude and shape of angular signatures of the reflected radiation at the beginning and the end of our observation period have been detected. Similarly, no changes in the canopy spectral coefficient at all MISR spectral bands are found. These findings suggest no changes in structure and leaf optics of the Congolese forests before and after the observed drying event. Thus we conclude, MODIS NDVI, EVI and LAI long-term records and MISR angular signatures of forest reflected radiation show no signs of long-term drying impact on structure and leaf optics of the Congolese forests.

4. Discussion

Tropical rainforests play an essential role in modulating regional climate, surface energy balance and the Earth's carbon cycle (Chen et al., 2020; Cook et al., 2020). Understanding the seasonal and long-term variations in the structure and function of these ecosystems is crucial to prognosing their response to climate change (Bi et al., 2015). The equatorial central African rainforests, the second-largest on Earth after the Amazonian rainforests, is still lacking systematic analyses of its phenological behavior and interannual variation. The purpose of this study is to analyze seasonal changes and long-term trends in leaf area in intact and undisturbed regions of the Congolese rainforests (Supplementary Information Fig. S1) using remote sensing data from the past two decades. We focus on the analysis on three regions identified with normalized 20-year mean monthly climatology of precipitation, PAR and LAI by using a K-means clustering algorithm, an unsupervised measure to find similar features from multiple inputs (Fig. 2). This clustering technique also localizes a highland region in the southeast part (Region 4 in Fig. 2) that represents a montane ecosystem.

Monthly precipitation data from TRMM show a bimodal variation over the Congolese rainforest, suggesting two dry (December–January–February and June–July–August) and two wet (September–October–November and March–April–May) seasons (Fig. 3). This is consistent with other precipitation datasets, such as Global Precipitation Climatology Centre (GPCC), Global Precipitation Climatology Project (GPCP) and Climatic Research Unit (CRU) (Jiang et al., 2019; Raghavendra et al., 2020; Sorí et al., 2017). Monthly average LAI from MODIS and forest canopy reflectance from EPIC follow seasonal patterns of precipitation, with higher values during the wet seasons (Fig. 3). The PAR incident on the forest canopy also exhibits a bimodal pattern, although somewhat less distinct: clear-cut variations from December to October

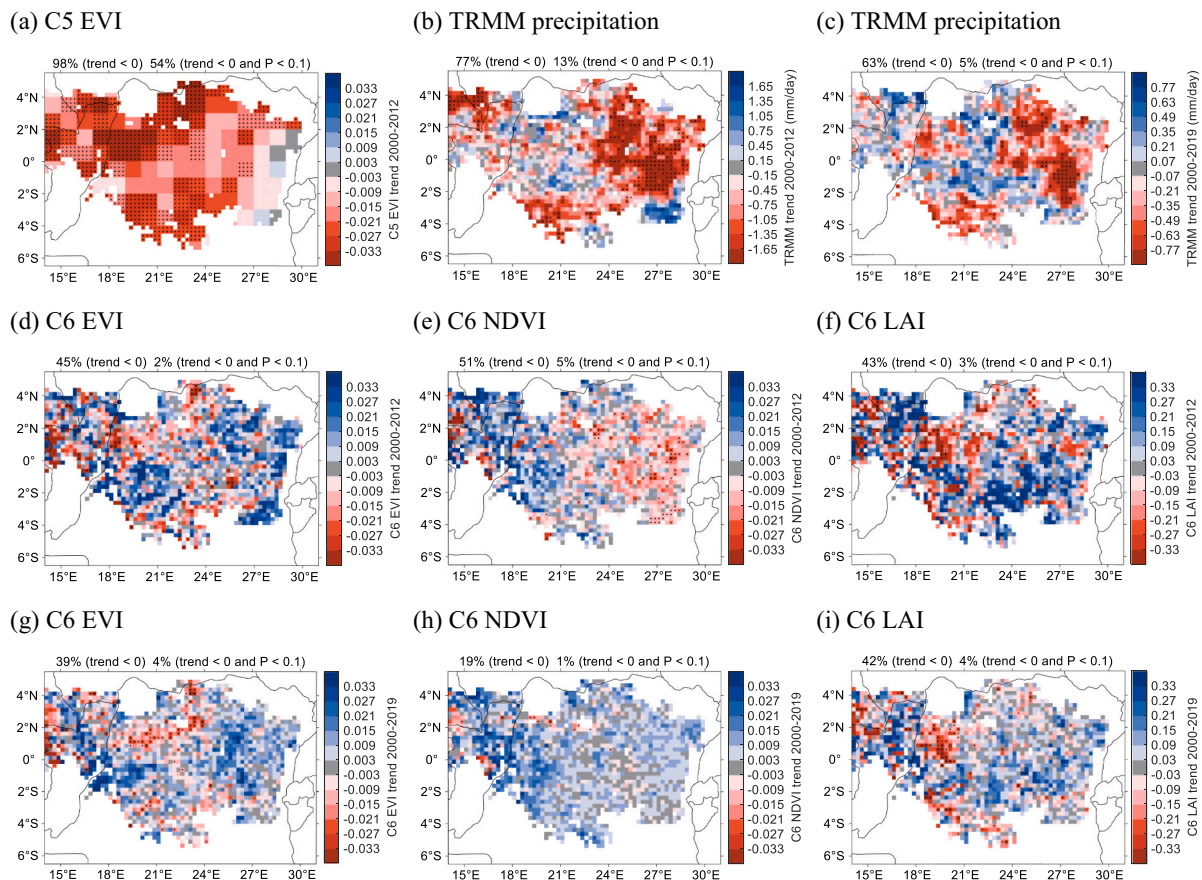


Fig. 6. Linear trends per decade in April-May-June for the period of 2000–2012 and 2000–2019. Pixels with the plus symbol indicate statistically significant trends ($P < 0.1$). Percentages of pixels with negative trends and negative trends at $P < 0.1$ are shown above each plot. The upper plots show trends in MODIS Collection 5 EVI from 2000 to 2012 (panel a) and TRMM precipitations for the 2000 to 2012 (panel b) and 2000 to 2019 (panel c) periods. Trends in MODIS Collection 6 EVI, NDVI and LAI for the 2000 to 2012 and the 2000 to 2019 periods are shown in middle and lower plots, respectively.

and a weaker oscillation from October to December. Sub-seasonal cycle from December to May shows less precipitation and more PAR, while the cycle from June to December has more precipitation and less PAR (Fig. 3). The bimodal patterns vary latitudinally with the amplitude increasing from North to South (Fig. 3).

The MODIS LAI values used in this research are mostly retrieved under the condition of reflectance saturation. The seasonality of satellite data-based LAI may therefore result from a decreased retrieval accuracy and/or variation in sun-satellite sensor geometry (Galvão et al., 2011; Morton et al., 2014). We develop a new approach that allows us to unambiguously detect changes in properties of the Congolese rainforest using angular variation of forest BRF as a source of diagnostic information. This methodology is applied to obtained independent observational evidence from MISR and EPIC data in support of the validity of the satellite derived seasonal variation in leaf area. Angular variations of forest DASF and canopy reflectance observed by the MISR and EPIC sensors clearly show seasonal increases and decreases in the amount of radiation reflected by the Congolese forests in all directions simultaneously (Fig. 4; Supplementary Information Fig. S5). Such changes can only be attributed to corresponding seasonal increases and decreases of LAI. This corroborates the seasonal behavior of leaf area derived from the MODIS observations. We also find that the canopy scattering coefficient exhibits an opposite tendency: its value increases from wet to dry and decreases from dry to wet seasons in the Congolese rainforests (Fig. 4, right panels). Similar tendencies were also found in Amazonian rainforests (Köhler et al., 2018). Such variation can be linked to variation in the concentrations of chlorophyll and/or dry matter in green leaves (Supplementary Information Fig. S6). In summary, our approach

based on exploiting angular variation of forest reflected radiation as a source of diagnostic information, rooted in physics of radiative transfer, allows us to unambiguously detect changes in canopy structure and leaf optics. This undoubtedly offers the benefit of greater reliability of our conclusion.

A significant positive correlation between precipitation and LAI is observed for our study area and seasonal cycles (Table 2). The time series of 20-year monthly precipitation and LAI over the Congolese forests are significantly positively correlated ($R = 0.67$, $P < 0.01$, Fig. S7). Whereas LAI and precipitation are always positively correlated, correlation between LAI and PAR can be both negative as during cycle 1 in regions 1 and 2 and positive as in cycle 2 (Table 2). These findings suggest that the observed seasonality of LAI is mainly controlled by precipitation in the Congolese rainforests (Gond et al., 2013; Yan et al., 2016a), as contrast to its Amazonian counterpart, where LAI is positive correlated with PAR (Bi et al., 2015; Brando et al., 2010; Huete et al., 2006; Myneni et al., 2007). Abundant annual precipitation (2332 mm yr^{-1}) creates a well-hydrated environmental condition in the Amazonian rainforests (Yang et al., 2018a), thus the water is not a main limitation and higher leaf area appears during the sunlight-rich dry season. A decrease in annual precipitation (1775 mm yr^{-1}) makes the leaf flushing and photosynthesis in the Congolese rainforests more dependent on water supply, especially in dry season when the monthly precipitation can fall below 90 mm (Fig. 1). Less solar radiation during the dry season (Figure 1 and Supplementary Information Fig. S3) may lead to lower leaf area in the Congolese rainforests. This, however, can only explain LAI decrease in dry season 2 (JJA). In addition, a low-level cloudiness developing during the dry season 2 causes high quality of

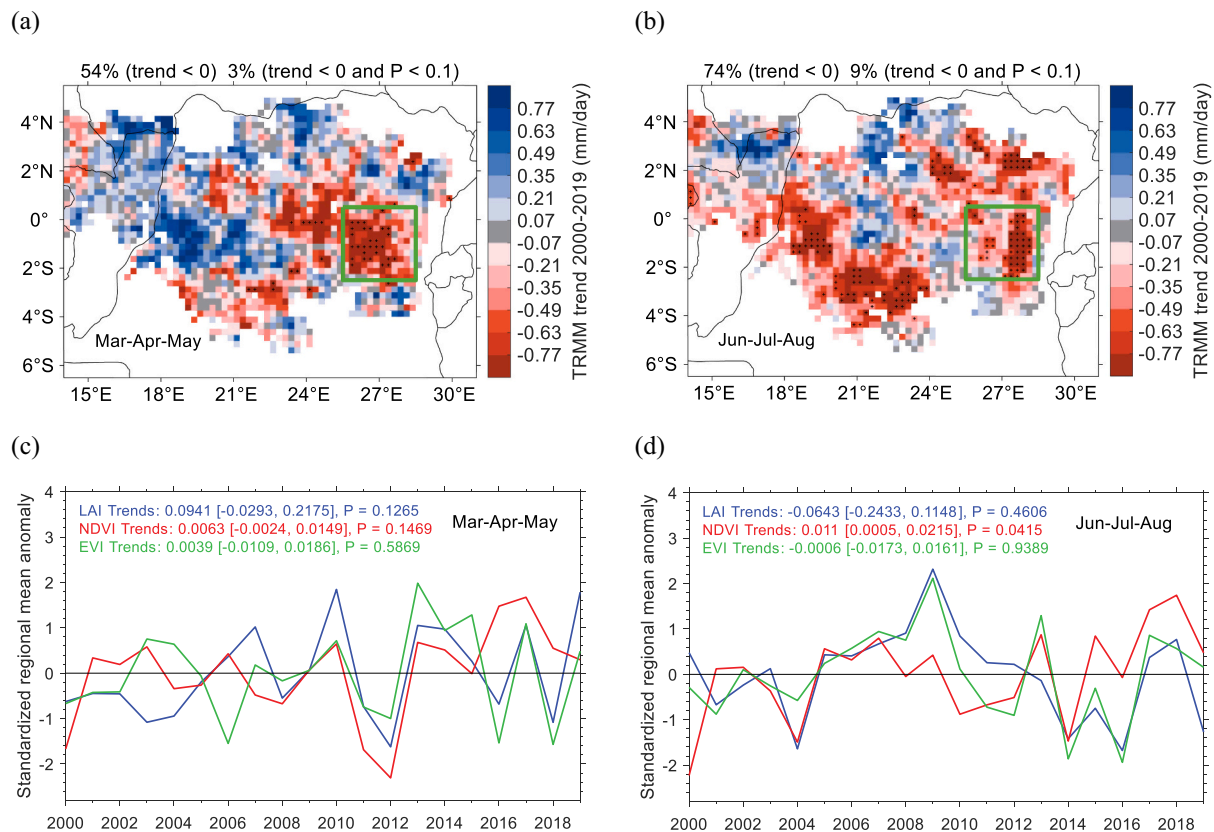


Fig. 7. Upper panels. Precipitation linear trends per decade during (a) wet season 1 (MAM) and (b) dry season 2 (JJA) for the period of 2000–2019. Pixels with the plus symbols indicate statistically significant trends ($P < 0.1$). A region between 0.5°N – 2.5°S and 25.5°E – 28.5°E where a significant precipitation decline was observed both during the wet and dry seasons is shown as a green rectangle. Lower panels. Standardized regional mean anomalies in LAI, NDVI and EVI for the selected region during (c) wet (MAM) and (d) dry (JJA) seasons for the 2000–2019 period. The linear trend (with 95% confidence interval) per decade and its significance level P are shown in legends. (For interpretation of the references to colour in this figure legend, the reader is referred to the web version of this article.)

light that sustain a more efficient photosynthesis (Mercado et al., 2009; Philippon et al., 2019), which should benefit leaf area growing. Hence, water supply is believed as the main limitation for seasonal leaf area variation. From the ecological perspective, the difference in the total annual precipitation and its diverse intra-annual variability strongly influence phenological behavior of rainforests and other vegetation types in the tropical regions (Ndehedehe et al., 2019; Yan et al., 2017).

Distinct spatiotemporal dependence of leaf area sensitivity to the seasonal variation in precipitation is observed in the Congo basin. The sensitivity of LAI to changes in precipitation tends to decrease from north to south for the full seasonal cycle (December to November, Fig. 5a). The phenological regions (Fig. 2) show weak variations of the sensitivity within a seasonal cycle (cf. Fig. 5b and c). LAI exhibits a stronger response to changes in precipitation from December to June compared to the second seasonal cycle (June to November). This difference is attributed to very different distributions of precipitation, PAR and climatic water deficit during the two seasonal cycles (Supplementary Information Fig. S8). Note that only very few factors were accounted for in our analyses. Further analyses of combined effects of precipitation, PAR, and other factors are needed to obtain a comprehensive insight into the causes of leaf area seasonal variation. Besides, a better understanding of the phenological response of Congolese rainforests depends on further in situ studies as satellite data can only complement but not substitute field data.

A widespread decline in Congolese rainforest greenness over the 2000–2012 period has been recently reported (Jiang et al., 2019; Raghavendra et al., 2020; Zhou et al., 2014). This result however was questioned, suggesting no significant browning signal in the 2000 to 2017 period (Chen et al., 2019; Piao et al., 2020). These contradictory

results justify a re-examination of the long-term trend in greenness of the Congolese forests.

We reproduce their result using the same Terra MODIS C5 EVI data (Fig. 6, upper panels), which is then compared to that from the latest MODIS C6 EVI dataset. We find that the widespread decline of Congo rainforest greenness disappear in the latest C6 MODIS data (Fig. 6, middle and lower panels): only 2% to 3% of the forests show significant negative trends in EVI, NDVI and LAI ($P < 0.1$) compared to 54% ($P < 0.1$) decline in EVI reported in (Zhou et al., 2014). The difference in the trends detected by C5 and C6 EVIs is attributed to the Terra MODIS sensor degradation for the period after 2007 (Lyapustin et al., 2014; Wang et al., 2012; Zhang et al., 2017). Moreover, a significant increase in total aerosols over the Congolese rainforests within the last decade has been detected (Moparthy et al., 2019). This can amplify the apparent long-term trends of canopy greenness these changes in aerosol loads are not correctly taken into account. C6 data reprocessing has significantly alleviated these problems (Detsch et al., 2016; Zhang et al., 2017) and made the result more credible.

A significant precipitation decline has been observed in the South-East part of our study area (Figs. 7a and b). However, no significant decline or increase in trends in regional mean NDVI, EVI and LAI over the past two decades are detected (Figs. 7c and d). The time series of LAI and EVI are found to be strongly correlated with $R = 0.56$ ($P < 0.01$) during wet (March–April–May) and $R = 0.74$ ($P < 0.01$) during dry (June–July–August) seasons. We also find no significant differences in magnitude and shape of angular distribution of forest reflected radiation and leaf optics at the beginning and the end of our observation period (Fig. 8). Thus, MODIS NDVI, EVI and LAI long-term records and MISR angular signatures of forest reflected radiation show no signs of drying

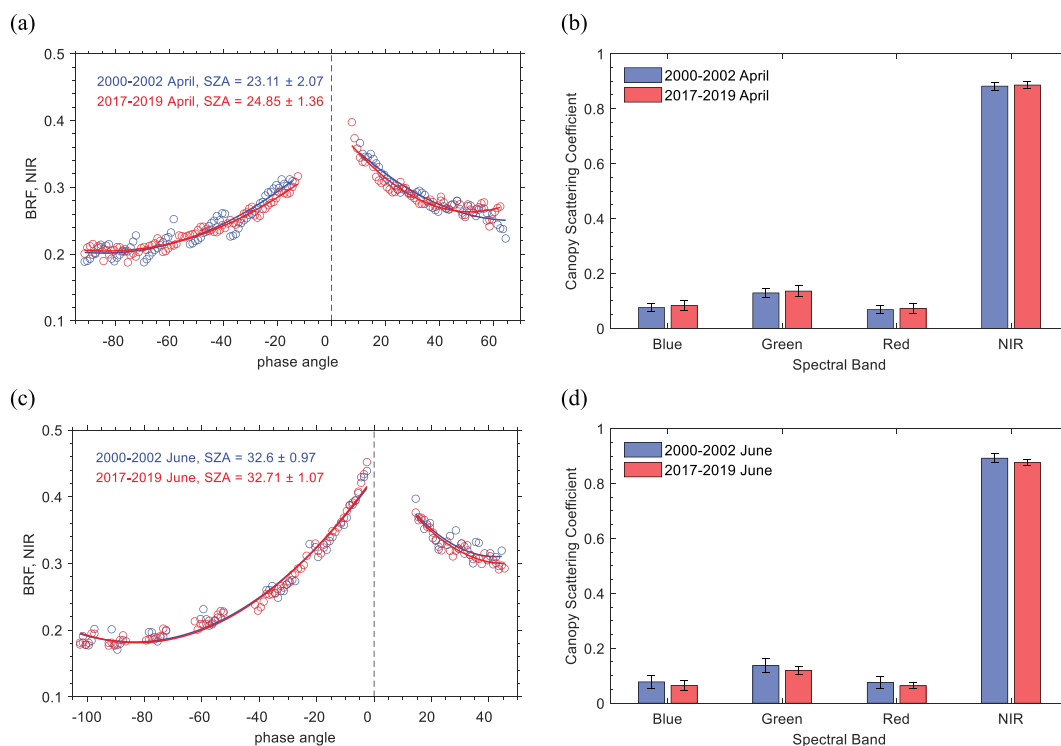


Fig. 8. MISR BRF at NIR (866 nm) and canopy scattering coefficient (right panels) of the region with significant drought at the beginning (2000–2002) and at the end (2017–2019) of the 2000–2019 observation period. Upper and lower panels show BRF and the coefficient in April (wet season) and June (dry season), respectively. These variables other months show similar behavior.

impact on structure and leaf optics even in the South-East part of the Congolese forests where a significant drying is observed.

Long-term drying does not induce vegetation degradation, and possible explanations for the neutral response of leaf area to the declines in precipitations at the seasonal and inter-annual scales could be given as follows. First, the decrease in monthly precipitation under a long-term drying condition is much smaller compared to a wet-to-dry precipitation amplitude of about 219 mm to 86 mm (Fig. 1), which still can satisfy plant water demands. Dry frequency is not high enough to suppress compensation of water supply from other months or seasons, allowing the forest to endure precipitation deficit. Second, decades of long-term drying in the Congolese rainforests may result in more drought-adapted species compared with other tropical forests, and this adaptive mechanisms by utilization of soil water reserves can tolerate water deficit short-time events (Asefi-Najafabady and Saatchi, 2013; Borchert, 1998). Third, suitable climate conditions—slight temperature increase and climatic water deficit decline (Supplementary Information Fig. S10), may benefit the growth of vegetation (Li et al., 2019) and in turn offset the negative impact from precipitation decline. More comprehensive explorations, such as model-based study, on this debate are still needed in the future investigation to get a better understanding.

5. Conclusion

This study comprehensively evaluated the seasonality and long-term trends of leaf area in Congolese forests with multiple remotely sensed datasets. We found that the seasonal variations of leaf area from MODIS data co-vary with the bimodal precipitation pattern, with higher values during the wet season, and the bimodal patterns vary latitudinally within this large region. Angular reflectance signatures derived from MISR and EPIC data further corroborated this seasonal behavior of leaf area. Two sub-seasonal cycles, each consisting of a dry and wet season, exhibited different leaf area sensitivities to changes in precipitation. No widespread decline in leaf area was detected across the Congolese

rainforest over the past two decades with the latest MODIS C6 dataset. Long-term drying did happen in some local areas of Congolese forests; however, those had minimal impacts on leaf area detected from MODIS and MISR observations.

Declaration of Competing Interest

The authors declare that they have no known competing financial interests or personal relationships that could have appeared to influence the work reported in this paper.

Credit Author Statement

Yuanheng Sun: Conceptualization, Methodology, Software, Data Curation, Investigation, Visualization, Writing - Original Draft, Writing - Review & Editing. Yuri Knyazikhin: Methodology, Software, Writing - Original Draft, Writing - Review & Editing. Xiaojun She: Visualization, Investigation. Xiangnan Ni: Validation, Investigation. Chi Chen: Investigation, Formal analysis. Huazhong Ren: Investigation, Formal analysis. Ranga B. Myneni: Conceptualization, Supervision, Project administration.

Acknowledgment

This research was funded by grants from the Earth Science Division of the National Aeronautics and Space Administration. Y. Sun was also funded by the China Scholarship Council (201906010045). C. Chen acknowledges additional support from the U.S. Department of Energy, Office of Science Biological and Environmental Research, Reducing Uncertainties in Biogeochemical Interactions through Synthesis and Computation Scientific Focus Area.

Appendix A. Supplementary data

Supplementary data to this article can be found online at <https://doi.org/10.1016/j.rse.2021.112762>.

References

- Adams, H.D., Guardiola-Claramonte, M., Barron-Gafford, G.A., Villegas, J.C., Breshears, D.D., Zou, C.B., Troch, P.A., Huxman, T.E., 2009. Temperature sensitivity of drought-induced tree mortality portends increased regional die-off under global-change-type drought. *Proc. Natl. Acad. Sci.* 113 (106), 7063–7066.
- Aguirre-Gutiérrez, J., Malhi, Y., Lewis, S.L., Fauset, S., Adu-Bredu, S., Affum-Baffoe, K., Baker, T.R., Gvozdevaite, A., Hubau, W., Moore, S., Pehrah, T., Ziemnińska, K., Phillips, O.L., Oliveras, I., 2020. Long-term droughts may drive driver tropical forests towards increased functional, taxonomic and phylogenetic homogeneity. *Nat. Commun.* 11, 3346.
- Aragão, L.E.O.C., Anderson, L.O., Fonseca, M.G., Rosan, T.M., Vedovato, L.B., Wagner, F. H., Silva, C.V.J., Silva Junior, C.H.L., Arai, E., Aguiar, A.P., Barlow, J., Berenguer, E., Deeter, M.N., Domingues, L.G., Gatti, L., Gloor, M., Malhi, Y., Marengo, J.A., Miller, J.B., Phillips, O.L., Saatchi, S., 2018. 21st century drought-related fires counteract the decline of Amazon deforestation carbon emissions. *Nat. Commun.* 9, 536.
- Asefi-Najafabady, S., Saatchi, S., 2013. Response of African humid tropical forests to recent rainfall anomalies. *Philos. Trans. R. Soc. B-Biol. Sci.* 368, 20120306.
- Bi, J., Knyazikhin, Y., Choi, S., Park, T., Barichivich, J., Ciais, P., Fu, R., Ganguly, S., Hall, F., Hilker, T., Huete, A., Jones, M., Kimball, J., Lyapustin, A.I., Mottus, M., Nemani, R.R., Piao, S., Poulter, B., Saleska, S.R., Saatchi, S.S., Xu, L., Zhou, L., Myneni, R.B., 2015. Sunlight mediated seasonality in canopy structure and photosynthetic activity of Amazonian rainforests. *Environ. Res. Lett.* 10 (6).
- Borchert, R., 1998. Responses of tropical trees to rainfall seasonality and its long-term changes. *Clim. Chang.* 39, 381–393.
- Brando, P.M., Goetz, S.J., Baccini, A., Nepstad, D.C., Beck, P.S.A., Christman, M.C., 2010. Seasonal and interannual variability of climate and vegetation indices across the Amazon. *Proc. Natl. Acad. Sci.* 107, 14685–14690.
- Brienen, R.J.W., Phillips, O.L., Feldpausch, T.R., Gloor, E., Baker, T.R., Lloyd, J., Lopez-Gonzalez, G., Monteagudo-Mendoza, A., Malhi, Y., Lewis, S.L., Vásquez Martínez, R., Alexiades, M., Álvarez Dávila, E., Alvarez-Loayza, P., Andrade, A., Aragão, L.E.O.C., Araujo-Murakami, A., Arets, E.J.M.M., Arroyo, L., Aymard, C.G.A., Bánki, O.S., Baraloto, C., Barroso, J., Bonal, D., Boot, R.G.A., Camargo, J.L.C., Castilho, C.V., Chama, V., Chao, K.J., Chave, J., Comiskey, J.A., Cornejo Valverde, F., da Costa, L., de Oliveira, E.A., Di Fiore, A., Erwin, T.L., Fauset, S., Forsthofer, M., Galbraith, D.R., Grahame, E.S., Groot, N., Hérault, B., Higuchi, N., Honorio Coronado, E.N., Keeling, H., Killeen, T.J., Laurance, W.F., Laurance, S., Licona, J., Magnussen, W.E., Marimon, B.S., Marimon-Junior, B.H., Mendoza, C., Neill, D.A., Nogueira, E.M., Núñez, P., Pallqui Camacho, N.C., Parada, A., Pardo-Molina, G., Peacock, J., Peña-Claros, M., Pickavance, G.C., Pitman, N.C.A., Poorter, L., Prieto, A., Quesada, C.A., Ramírez, F., Ramírez-Angulo, H., Restrepo, Z., Roopsind, A., Rudas, A., Salomão, R. P., Schwarz, M., Silva, N., Silva-Espejo, J.E., Silveira, M., Stropp, J., Talbot, J., ter Steege, H., Teran-Aguilar, J., Terborgh, J., Thomas-Caesar, R., Toledo, M., Torello-Raventos, M., Umetsu, R.K., van der Heijden, G.M.F., van der Hout, P., Guimarães Vieira, I.C., Vieira, S.A., Vilanova, E., Vos, V.A., Zagt, R.J., 2015. Long-term decline of the Amazon carbon sink. *Nature* 519, 344–348.
- Celik, T., 2009. Unsupervised change detection in satellite images using principal component analysis and k-means clustering. *IEEE Geosci. Remote Sens. Lett.* 6, 772–776.
- Chen, C., Li, D., Li, Y., Piao, S., Wang, X., Huang, M., Gentile, P., Nemani, R.R., Myneni, R.B., 2020. Biophysical impacts of earth greening largely controlled by aerodynamic resistance. *Science advances* 6 (47), eabb1981.
- Chen, C., Park, T., Wang, X., Piao, S., Xu, B., Chaturvedi, R.K., Fuchs, R., Brovkin, V., Ciais, P., Fensholt, R., Tommervik, H., Bala, G., Zhu, Z., Nemani, R.R., Myneni, R.B., 2019. China and India lead in greening of the world through land-use management. *Nat. Sustain.* 2, 122–129.
- Cook, K.H., Liu, Y., Vizy, E.K., 2020. Congo Basin drying associated with poleward shifts of the African thermal lows. *Clim. Dyn.* 54, 863–883.
- Costa, M.H., Yanagi, S.N.M., Souza, P.J.O.P., Ribeiro, A., Rocha, E.J.P., 2007. Climate change in Amazonia caused by soybean cropland expansion, as compared to caused by pastureland expansion. *Geophys. Res. Lett.* p. 34.
- Detsch, F., Insa, O., Appelhans, T., Naus, T., 2016. A comparative study of cross-product NDVI dynamics in the Kilimanjaro region—A matter of sensor, degradation calibration, and significance. *Remote Sens.* 8.
- Fauset, S., Baker, T.R., Lewis, S.L., Feldpausch, T.R., Affum-Baffoe, K., Foli, E.G., Hamer, K.C., Swaine, M.D., 2012. Drought-induced shifts in the floristic and functional composition of tropical forests in Ghana. *Ecol. Lett.* 15, 1120–1129.
- Féret, J.B., Francois, C., Asner, G.P., Gitelson, A.A., Martin, R.E., Bidel, L.P.R., Ustin, S.L., le Maire, G., Jacquemoud, S., 2008. PROSPECT-4 and 5: advances in the leaf optical properties model separating photosynthetic pigments. *Remote Sens. Environ.* 112, 3030–3043.
- Friedl, M.A., McIver, D.K., Hodges, J.C.F., Zhang, X.Y., Muchoney, D., Strahler, A.H., Woodcock, C.E., Gopal, S., Schneider, A., Cooper, A., Baccini, A., Gao, F., Schaaf, C., 2002. Global land cover mapping from MODIS: algorithms and early results. *Remote Sens. Environ.* 83, 287–302.
- Galvão, L.S., dos Santos, J.R., Roberts, D.A., Breunig, F.M., Toomey, M., de Moura, Y.M., 2011. On intra-annual EVI variability in the dry season of tropical forest: A case study with MODIS and hyperspectral data. *Remote Sens. Environ.* 115, 2350–2359.
- Gond, V., Fayolle, A., Penne, A., Cornu, G., Mayaux, P., Camberlin, P., Doumenge, C., Fauvet, N., Gourlet-Fleury, S., 2013. Vegetation structure and greenness in Central Africa from Modis multi-temporal data. *Philos. Trans. R. Soc. B-Biol. Sci.* 368, 20120309.
- Guan, K., Pan, M., Li, H., Wolf, A., Wu, J., Medvigy, D., Caylor, K.K., Sheffield, J., Wood, E.F., Malhi, Y., Liang, M., Kimball, J.S., Saleska, Scott R., Berry, J., Joiner, J., Lyapustin, A.I., 2015. Photosynthetic seasonality of global tropical forests constrained by hydroclimate. *Nat. Geosci.* 8, 284–289.
- Hirota, M., Holmgren, M., Van Nes, E.H., Scheffer, M., 2011. Global resilience of tropical Forest and savanna to critical transitions. *Science* 334, 232–235.
- Hua, W., Zhou, L., Chen, H., Nicholson, S.E., Jiang, Y., Raghavendra, A., 2018. Understanding the central equatorial African long-term drought using AMIP-type simulations. *Clim. Dyn.* 50, 1115–1128.
- Hua, W., Zhou, L., Chen, H., Nicholson, S.E., Raghavendra, A., Jiang, Y., 2016. Possible causes of the central equatorial African long-term drought. *Environ. Res. Lett.* 11, 124002.
- Huang, D., Knyazikhin, Y., Dickinson, R.E., Rautiainen, M., Stenberg, P., Disney, M., Lewis, P., Cescatti, A., Tian, Y., Verhoef, W., Martonchik, J.V., Myneni, R.B., 2007. Canopy spectral invariants for remote sensing and model applications. *Remote Sens. Environ.* 106, 106–122.
- Huete, A., Didan, K., Miura, T., Rodriguez, E.P., Gao, X., Ferreira, L.G., 2002. Overview of the radiometric and biophysical performance of the MODIS vegetation indices. *Remote Sens. Environ.* 83, 195–213.
- Huete, A.R., Didan, K., Shimabukuro, Y.E., Ratana, P., Saleska, S.R., Hutya, L.R., Yang, W., Nemani, R.R., Myneni, R., 2006. Amazon rainforests green-up with sunlight in dry season. *Geophys. Res. Lett.* 33.
- Huffman, G.J., Bolvin, D.T., Nelkin, E.J., Wolff, D.B., Adler, R.F., Gu, G., Hong, Y., Bowman, K.P., Stocker, E.F., 2007. The TRMM multisatellite precipitation analysis (TMPA): quasi-global, multiyear, combined-sensor precipitation estimates at fine scales. *J. Hydrometeorol.* 8, 38–55.
- Jacquemoud, S., Verhoef, W., Baret, F., Bacour, C., Zarco-Tejada, P.J., Asner, G.P., François, C., Ustin, S.L., 2009. PROSPECT+SAIL models: A review of use for vegetation characterization. *Remote Sens. Environ.* 113, S56–S66.
- Jiang, Y., Zhou, L., Tucker, C.J., Raghavendra, A., Hua, W., Liu, Y.Y., Joiner, J., 2019. Widespread increase of boreal summer dry season length over the Congo rainforest. *Nat. Clim. Chang.* 9, 617–622.
- Knyazikhin, Y., Schull, M., Xu, L., Myneni, R., Samanta, A., 2011. Canopy spectral invariants. Part 1: A new concept in remote sensing of vegetation. *J. Quant. Spectrosc. Radiat. Transf.* 112, 727–735.
- Knyazikhin, Y., Schull, M.A., Stenberg, P., Mottus, M., Rautiainen, M., Yang, Y., Marshak, A., Latorre Carmona, P., Kaufmann, R.K., Lewis, P., Disney, M.I., Vanderbilt, V., Davis, A.B., Baret, F., Jacquemoud, S., Lyapustin, A., Myneni, R.B., 2013. Hyperspectral remote sensing of foliar nitrogen content. *Proc. Natl. Acad. Sci.* 110, E185–E192.
- Köhler, P., Guanter, L., Kobayashi, H., Walther, S., Yang, W., 2018. Assessing the potential of sun-induced fluorescence and the canopy scattering coefficient to track large-scale vegetation dynamics in Amazon forests. *Remote Sens. Environ.* 204, 769–785.
- Lewis, P., Disney, M.I., 2007. Spectral invariants and scattering across multiple scales from within-leaf to canopy. *Remote Sens. Environ.* 109, 196–206.
- Li, W., Du, J., Li, S., Zhou, X., Duan, Z., Li, R., Wu, S., Wang, S., Li, M., 2019. The variation of vegetation productivity and its relationship to temperature and precipitation based on the GLASS-LAI of different African ecosystems from 1982 to 2013. *Int. J. Biometeorol.* 63, 847–860.
- Liu, H.Q., Huete, A., 1995. A feedback based modification of the NDVI to minimize canopy background and atmospheric noise. *IEEE Trans. Geosci. Remote Sens.* 33, 457–465.
- Lyapustin, A., Wang, Y., Xiong, X., Meister, G., Platnick, S., Levy, R., Franz, B., Korkin, S., Hilker, T., Tucker, J., Hall, F., Sellers, P., Wu, A., Angal, A., 2014. Scientific impact of MODIS C5 calibration degradation and C6+ improvements. *Atmos. Meas. Tech.* 7, 4353–4365.
- Marshak, A., Knyazikhin, Y., 2017. The spectral invariant approximation within canopy radiative transfer to support the use of the EPIC/DSCOVR oxygen B-band for monitoring vegetation. *J. Quant. Spectrosc. Radiat. Transf.* 191, 7–12.
- Martínez-Vilalta, J., Lloret, F., 2016. Drought-induced vegetation shifts in terrestrial ecosystems: the key role of regeneration dynamics. *Glob. Planet. Chang.* 144, 94–108.
- Mercado, L.M., Bellouin, N., Stith, S., Boucher, O., Huntingford, C., Wild, M., Cox, P.M., 2009. Impact of changes in diffuse radiation on the global land carbon sink. *Nature* 458, 1014–1017.
- Moparty, S., Carrer, D., Ceamanos, X., 2019. Can we detect the brownness or greenness of the Congo rainforest using satellite-derived surface albedo? A study on the role of aerosol uncertainties. *Sustainability* 11, 1410.
- Morton, D.C., Nagol, J., Carabajal, C.C., Rosette, J., Palace, M., Cook, B.D., Vermote, E.F., Harding, D.J., North, P.R.J., 2014. Amazon forests maintain consistent canopy structure and greenness during the dry season. *Nature* 506, 221–224.
- Mu, Q., Heinsch, F.A., Zhao, M., Running, S.W., 2007. Development of a global evapotranspiration algorithm based on MODIS and global meteorology data. *Remote Sens. Environ.* 111, 519–536.
- Mu, Q., Zhao, M., Running, S.W., 2011. Improvements to a MODIS global terrestrial evapotranspiration algorithm. *Remote Sens. Environ.* 115, 1781–1800.
- Myneni, R.B., Yang, W., Nemani, R.R., Huete, A.R., Dickinson, R.E., Knyazikhin, Y., Didan, K., Fu, R., Negrón Juárez, R.I., Saatchi, S.S., Hashimoto, H., Ichii, K., Shabanov, N.V., Tan, B., Ratana, P., Privette, J.L., Morissette, J.T., Vermote, E.F., Roy, D.P., Wolfe, R.E., Friedl, M.A., Running, S.W., Votava, P., El-Saleous, N.,

- Devadiga, S., Su, Y., Salomonson, V.V., 2007. Large seasonal swings in leaf area of Amazon rainforests. *Proc. Natl. Acad. Sci.* 104, 4820–4823.
- Ndehedehe, C.E., Ferreira, V.G., Agutu, N.O., 2019. Hydrological controls on surface vegetation dynamics over west and Central Africa. *Ecol. Indic.* 103, 494–508.
- Nicholson, S.E., 2018. The ITCZ and the seasonal cycle over equatorial Africa. *Bull. Am. Meteorol. Soc.* 99, 337–348.
- Oliveira, R.S., Dawson, T.E., Burgess, S.S.O., Nepstad, D.C., 2005. Hydraulic redistribution in three Amazonian trees. *Oecologia* 145, 354–363.
- Philippou, N., Cornu, G., Monteil, L., Gond, V., Moron, V., Pergaud, J., Sèze, G., Bigot, S., Camberlin, P., Doumenge, C., Fayolle, A., Ngomanda, A., 2019. The light-deficient climates of western central African evergreen forests. *Environ. Res. Lett.* 14, 034007.
- Piao, S., Wang, X., Park, T., Chen, C., Lian, X., He, Y., Bjerke, J.W., Chen, A., Ciais, P., Tømmervik, H., Nemani, R.R., Myneni, R.B., 2020. Characteristics, drivers and feedbacks of global greening. *Nature Reviews Earth & Environment* 1, 14–27.
- Pierret, A., Maeght, J.-L., Clément, C., Montoroi, J.-P., Hartmann, C., Gonkhamdee, S., 2016. Understanding deep roots and their functions in ecosystems: an advocacy for more unconventional research. *Ann. Bot.* 118, 621–635.
- Pires, G.F., Costa, M.H., 2013. Deforestation causes different subregional effects on the Amazon bioclimatic equilibrium. *Geophys. Res. Lett.* 40, 3618–3623.
- Raghavendra, A., Zhou, L., Jiang, Y., Hua, W., 2018. Increasing extent and intensity of thunderstorms observed over the Congo Basin from 1982 to 2016. *Atmos. Res.* 213, 17–26.
- Raghavendra, A., Zhou, L., Roundy, P.E., Jiang, Y., Milrad, S.M., Hua, W., Xia, G., 2020. The MJO's impact on rainfall trends over the Congo rainforest. *Clim. Dyn.* 54, 2683–2695.
- Rouse, J.W., Haas, R.H., Schell, J.A., Deering, D.W., 1974. Monitoring vegetation Systems in the Great Plains with ERTS. In: *Third Earth Resources Technology Satellite-1 Symposium- Volume I: Technical Presentations*. NASA, Washington, D.C.
- Rutan, D.A., Kato, S., Doelling, D.R., Rose, F.G., Nguyen, L.T., Caldwell, T.E., Loeb, N.G., 2015. CERES synoptic product: methodology and validation of surface radiant flux. *J. Atmos. Ocean. Technol.* 32, 1121–1143.
- Samanta, A., Knyazikhin, Y., Xu, L., Dickinson, R.E., Fu, R., Costa, M.H., Saatchi, S.S., Nemani, R.R., Myneni, R.B., 2012. Seasonal Changes in Leaf Area of Amazon Forests from Leaf Flushing and Abscission. *J. Geophys. Res.-Biogeosci.* 117 (G1).
- Song, W., Knyazikhin, Y., Wen, G., Marshak, A., Möttus, M., Yan, K., Yang, B., Xu, B., Park, T., Chen, C., 2018. Implications of whole-disc DSCOVR EPIC spectral observations for estimating Earth's spectral reflectivity based on low-earth-orbiting and geostationary observations. *Remote Sens.* 10, 1594.
- Sorí, R., Nieto, R., Vicente-Serrano, S.M., Drumond, A., Gimeno, L., 2017. A Lagrangian perspective of the hydrological cycle in the Congo River basin. *Earth Syst. Dynam.* 8, 653–675.
- Wan, Z., 2014. New refinements and validation of the collection-6 MODIS land-surface temperature/emissivity product. *Remote Sens. Environ.* 140, 36–45.
- Wang, D., Morton, D., Masek, J., Wu, A., Nagol, J., Xiong, X., Levy, R., Vermote, E., Wolfe, R., 2012. Impact of sensor degradation on the MODIS NDVI time series. *Remote Sens. Environ.* 119, 55–61.
- Wang, Y., Buermann, W., Stenberg, P., Smolander, H., Hame, T., Tian, Y., Hu, J., Knyazikhin, Y., & Myneni, R.B., 2003. A new parameterization of canopy spectral response to incident solar radiation: case study with hyperspectral data from pine dominant forest. *Remote Sens. Environ.* 85, 304–315.
- Xu, L., Saatchi, S.S., Yang, Y., Myneni, R.B., Frankenberg, C., Chowdhury, D., Bi, J., 2015. Satellite observation of tropical forest seasonality: spatial patterns of carbon exchange in Amazonia. *Environ. Res. Lett.* 10, 084005.
- Xu, L., Samanta, A., Costa, M.H., Ganguly, S., Nemani, R.R., Myneni, R.B., 2011. Widespread decline in greenness of Amazonian vegetation due to the 2010 drought. *Geophys. Res. Lett.* 38.
- Yan, D., Zhang, X., Yu, Y., Guo, W., 2016a. A comparison of tropical rainforest phenology retrieved from geostationary (SEVIRI) and polar-orbiting (MODIS) sensors across the Congo Basin. *IEEE Trans. Geosci. Remote Sens.* 54, 4867–4881.
- Yan, D., Zhang, X., Yu, Y., Guo, W., 2017. Characterizing land cover impacts on the responses of land surface phenology to the rainy season in the Congo Basin. *Remote Sens.* 9, 461.
- Yan, K., Park, T., Yan, G., Chen, C., Yang, B., Liu, Z., Nemani, R.R., Knyazikhin, Y., Myneni, R.B., 2016b. Evaluation of MODIS LAI/FPAR product collection 6. Part 1: consistency and improvements. *Remote Sens.* 8, 359.
- Yan, K., Park, T., Yan, G., Liu, Z., Yang, B., Chen, C., Nemani, R.R., Knyazikhin, Y., Myneni, R.B., 2016c. Evaluation of MODIS LAI/FPAR product collection 6. Part 2: validation and intercomparison. *Remote Sens.* 8, 460.
- Yang, B., Knyazikhin, Y., Mottus, M., Rautiainen, M., Stenberg, P., Yan, L., Chen, C., Yan, K., Choi, S., Park, T., Myneni, R.B., 2017. Estimation of leaf area index and its sunlit portion from DSCOVR EPIC data: theoretical basis. *Remote Sens. Environ.* 198, 69–84.
- Yang, J., Tian, H., Pan, S., Chen, G., Zhang, B., Dangal, S., 2018a. Amazon drought and forest response: largely reduced forest photosynthesis but slightly increased canopy greenness during the extreme drought of 2015/2016. *Glob. Chang. Biol.* 24, 1919–1934.
- Yang, Y., Saatchi, S.S., Xu, L., Yu, Y., Choi, S., Phillips, N., Kennedy, R., Keller, M., Knyazikhin, Y., Myneni, R.B., 2018b. Post-drought decline of the Amazon carbon sink. *Nat. Commun.* 9, 3172.
- Zhang, Y., Song, C., Band, L.E., Sun, G., Li, J., 2017. Reanalysis of global terrestrial vegetation trends from MODIS products: Browning or greening? *Remote Sens. Environ.* 191, 145–155.
- Zhou, L., Tian, Y., Myneni, R.B., Ciais, P., Saatchi, S., Liu, Y.Y., Piao, S., Chen, H., Vermote, E.F., Song, C., Hwang, T., 2014. Widespread decline of Congo rainforest greenness in the past decade. *Nature* 509, 86–90.